Product State Distributions of Vibrationally Excited CO(v) for the CH($X^2\Pi$) and CH($A^2\Delta$) Channels of the $C_2H + O(^3P)$ Reaction

Viktor Chikan, Boris Nizamov, and Stephen R. Leone*

Departments of Chemistry and Physics, and Lawrence Berkeley National Laboratory, University of California, Berkeley, California 94720-1460

Received: April 28, 2004; In Final Form: July 23, 2004

The $C_2H + O(^3P)$ reaction is investigated using time-resolved Fourier transform infrared spectroscopy (TR-FTIR). The C_2H and O radicals are produced by 193-nm photolysis of C_2H_2 and SO_2 precursors. Multiple vibrationally excited products are observed from several resulting reaction processes, including products: CO, CO_2, C_4H_2, and CH. For this choice of photolytic precursors, it is observed that the $C_2H + SO_2$, $C_2H_2 + O$, and the HCCO + O reactions contribute to the observed product signals. To evaluate the contribution of the $C_2H + SO_2$ reaction to the removal kinetics of C_2H in the C_2H_2/SO_2 system, the room-temperature rate constant for the $C_2H + SO_2$ reaction is experimentally determined to be $k = (1.1 \pm 0.3) \times 10^{-11}$ cm^3 molecule^{-1} s^{-1}. The time dependencies of the CO and CO_2 species are measured experimentally and simulated to determine conditions under which contributions from the several processes that give the same product can be differentiated. Analysis of the nascent vibrational distribution of the CO products from $C_2H + O$ suggests the participation of both CH($A^2\Delta$) and CH($X^2\Pi$) products, in the ratio of ∼3:2. The surprisal parameters for the vibrational distribution of the CO products of these two channels are found to be -1.5 ± 0.2 and -1.1 ± 0.2, respectively. It is suggested that the reaction proceeds through the HCCO‡ intermediate, in agreement with earlier studies, but the CH($A^2\Delta$)/CH($X^2\Pi$) branching fraction may be larger than previously reported.

Introduction

The reactions of ethynyl radical (C_2H) play an important role in combustion processes, interstellar chemistry,[1−3] and planetary atmospheres.[4,5] The C_2H radical is highly reactive at both high and low temperatures with hydrocarbons,[4,6−14] nitriles,[15,16] and O_2.[17] In high-temperature combustion, the C_2H radical is formed through various processes such as H-atom abstraction reactions from C_2H_2 or C_3H_x ($x = 1-3$) species by O or OH radicals.[18] It has been shown previously that the intense emission of hydrocarbon flames is partially due to the $C_2H + O_2$ reaction.[19−21] However, the rate constant of the $C_2H + O_2$ reaction alone cannot adequately account for all of the observed CH($A^2\Delta$) in C_2H_2/O_2 systems.[22] Devriendt et al.[22,23] established that the intense emission of hydrocarbon flames at 430 nm is in large part due to the $C_2H + O(^3P)$ reaction. In that work, the reaction of these two radicals was investigated by using a pulsed-laser photolysis/visible chemiluminescence technique, and it was found that the direct reaction of these two radicals produces CH($A^2\Delta$). The short emission lifetime of the CH($A^2\Delta$) state makes it very convenient to follow the $C_2H + O$ reaction. On the basis of that time-resolved visible emission data,[22,23] it was estimated first that about 30% of the $C_2H + O(^3P)$ reaction proceeds through the CH($A^2\Delta$) + CO channel of all possible channels. However, because of the uncertainty of the C_2H quantum yield, the branching fraction for the CH($A^2\Delta$) channel was later revised, and an updated, much smaller value was reported of ∼8%.[24] Peeters et al. also showed[25] that there is a possibility that the $C_2H + O(^3P)$ reaction proceeds through the formation of the CH($a^4\Sigma^-$) radical and CO. This channel was shown to be of relatively little importance compared to the other channels.

There are many possible channels for the $C_2H + O(^3P)$ reaction as shown below, but only four of them are exothermic

$$C_2H(X^2\Sigma^+) + O(^3P) \rightarrow CO + CH(X^2\Pi) \quad (-76.5 \text{ kcal/mol}) \quad \text{(R1)}$$

$$\rightarrow CO + CH(A^2\Delta) \quad (-10.5 \text{ kcal/mol}) \quad \text{(R2)}$$

$$\rightarrow CO + CH(a^4\Sigma^-) \quad (-59.8 \text{ kcal/mol})$$

$$\rightarrow HCCO \ (-140 \text{ kcal/mol})$$

$$\rightarrow C_2 + OH \quad (71 \text{ kcal/mol})$$

$$\rightarrow C_2O + H \quad (187 \text{ kcal/mol})$$

Most of the previous studies[22,23] of this reaction focused on the channel that produces CH($A^2\Delta$) radicals. It is presumed that HCCO is not stabilized at low pressure, and the branching ratio for the CH($a^4\Sigma^-$) channel is negligible. Therefore, the CH($X^2\Pi$) and CH($A^2\Delta$) products are the major pathways.

The purpose of this paper is to explore the mechanism of the $C_2H + O(^3P)$ reaction by observing emission from the vibrationally excited products of this reaction. This study uses the TR-FTIR technique to obtain both time- and state-resolved information about the reaction products. The 193 nm photolysis of SO_2 and C_2H_2 is used to generate the $O(^3P)$ and C_2H radicals, respectively. The C_2H radical is commonly produced[26] by 193 nm photolysis of acetylene, bromoacetylene, or CF_3CCH. The 193 nm photodissociation pathways of acetylene are well established,[27−30] and they result in a mixture of ground electronic state C_2H radical and its low-lying first excited electronic state

* To whom all correspondence should be addressed.

10.1021/jp040317b CCC: $27.50
Published on Web 11/13/2004

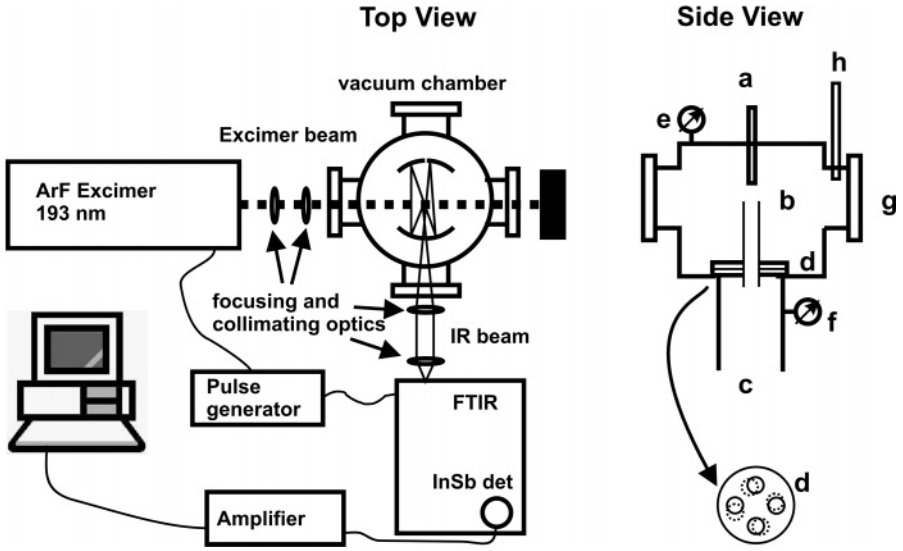

Figure 1. Simplified schematic diagram of the time-resolved FTIR apparatus used in this study. The gas is introduced through an effusive source perpendicular to the plane of the schematic diagram at the middle of the vacuum chamber. The excimer laser beam path is indicated by a dashed line. The right side of the figure shows the side view of the vacuum chamber. (part a) effusive source, (part b) skimmer to confine the gas flow into the observation zone, (part c) large-diameter tube to the pump, (part d) rotatable base plate to regulate pumping speed, (parts e−f) pressure gauges, (part g) entrance window for excimer laser, (part h) buffer gas inlet.

($C_2H(\tilde{A}^2\Delta)$).[28,31] In the C_2H_2/SO_2 system, several vibrationally excited products are observed: CO, CH, CO_2, SO_2, and C_4H_2. Some of these products come from reactions other than $C_2H + O$, such as $C_2H_2 + O$ and $C_2H + SO_2$. Additionally, vibrationally excited CO can come from reactions such as $CH + O$; although the rate constant of this reaction is an order of magnitude faster than the rate constant for $C_2H + O$, it will be shown that it is of minor importance under the experimental conditions.

To obtain the nascent vibrational distributions from the $C_2H + O$ reaction, it was necessary to evaluate contributions from these interfering reactions. This was done by measuring the rate constant for the $C_2H + SO_2$ reaction and simulating the kinetics using available literature rate constants to achieve a better understanding of the kinetics initiated by 193 nm photolysis in the C_2H_2/SO_2 mixture. It is possible to determine the nascent vibrational distribution of the CO product from the $C_2H + O$ reaction under suitable conditions. This distribution shows a bimodal behavior. This vibrational distribution is parametrized in terms of surprisal parameters, which indicate nearly statistical distributions for both $CH(X^2\Pi) + CO(v)$ and $CH(A^2\Delta) + CO(v)$ channels. The large difference between the previously determined $CH(A^2\Pi)$ branching fraction (8%) and the branching fraction determined by extrapolation of these vibrational distributions (60%) for the $CH(A^2\Delta) + CO(v)$ channel suggests that this channel may be underestimated, or the vibrational distribution for the $CH(A^2\Delta)$ channel could be more inverted with respect to $v = 0$ than predicted by the linear surprisal extrapolation, or the $CO(v)$ from the $CH(X^2\Pi)$ channel has more contribution at lower v than that predicted by a linear surprisal. The significance of the observed vibrational distribution to understanding the mechanism of the $C_2H + O$ reaction is discussed.

Experimental Section

Time-resolved Fourier transform infrared emission spectroscopy[32] is a very useful and powerful technique to probe vibrationally excited reaction products and photoproducts. This technique can identify chemical species and monitor their kinetics at the same time. The method is particularly applicable to gas-phase reactions, where the state distribution of the excited photoproducts or reaction products can be determined from the rotationally and vibrationally resolved spectra. Analysis of the temporal evolution of the rovibrational spectra can reveal nascent rotational and vibrational distributions, providing important insights into reaction mechanisms.

Figure 1 shows a simplified diagram of the experimental apparatus used in this study. The reaction takes place in a vacuum chamber pumped by a 1000 L/s capacity Roots blower pump backed by an 80 L/s capacity mechanical pump. The reagents are introduced into the vacuum chamber through an effusive source, which consists of an ~1 cm i.d. stainless steel tube. In a perpendicular orientation to the reagent flow, an excimer laser beam enters into the vacuum chamber through a suprasil window and intersects the reagent flow approximately 1 cm below the effusive source to avoid scattered light from the excimer laser beam. The excitation source is a 193 nm ArF variable repetition rate excimer laser. The laser beam is focused to a 5 mm × 12 mm beam spot using cylindrical lenses. The average pulse energy is kept below 60−80 mJ/pulse in order to minimize the possibility of multiphoton processes and further absorption by the C_2H radical.[33] Earlier studies showed that, for laser fluences less than 100 mJ/cm^2, no excited C_2 radical can be observed as a result of photodissociation of the C_2H radical.[34] The IR radiation is collected by Welsh cell[35,36] optics and exits the vacuum chamber through a CaF_2 window.

Collected by the Welsh cell, the IR radiation is collimated and focused on the entrance port of a commercially available step-scan FTIR spectrometer, with optics to match its *f* number (4.5). An iris is placed in front of the spectrometer to reduce the field of view and achieve the desired spectral resolution. In the spectrometer, a CaF_2 (spectral range 1000−15 000 cm^{-1}) or KBr (spectral range 300−5000 cm^{-1}) beam splitter is chosen depending on the desired spectral range. The signal is detected by a liquid-nitrogen-cooled InSb or MCT detector. The InSb detector ($D^* \approx 2.2 \times 10^{11}$ cm Hz$^{1/2}$ W^{-1}, where D^* is detectivity) has higher sensitivity than the MCT detector ($D^* \cong 3.8 \times 10^{10}$ cm Hz$^{1/2}$ W^{-1}), but its response curve falls off at around 1800 cm^{-1}. The MCT detector has a better spectral range (lower limit ~1000 cm^{-1}), but it is not sensitive enough to get

high-resolution spectra within reasonable data acquisition times for this experiment. At each mirror step of the FTIR, the entire time history of the signal is recorded and coadded for 50−200 pulses to increase the signal-to-noise (*S*/*N*) ratio in the spectra. The maximum spectral resolution used in our experiments was measured to be ~0.2 cm^{-1}. The limiting factor determining the overall time resolution is the bandwidth of the low-noise, home-built current-to-voltage amplifier (250 kHz). The exponential time constant of the detector−amplifier combination used in the experiment is measured to be approximately 0.6 μs.

The C_2H radicals are generated by 193 nm photolysis of acetylene (99.6%), which is purified by an activated carbon trap in order to remove the residual acetone stabilizer from the C_2H_2 reagent flow. The trap is evacuated overnight before each experiment to ensure efficient removal of the acetone. The $O(^3P)$ is produced by photolysis of SO_2 (anhydrous, 99.98%). To ensure electronic relaxation of the photogenerated radicals, N_2, Ar, or He is used as a buffer gas. The buffer gas also helps keep the entrance window and the reflective surfaces of the Welsh cell optically clean and confines the reagent flow to the observation zone of the Welsh cell. Introduction of the buffer gas from outside the sample flow (see Figure 1) helps to confine the reagents to the observation zone, yielding a better *S*/*N* ratio. Pressure is measured using capacitance manometers. To get more accurate pressure measurement in the observation and interaction zone, the pressures are measured at several places in the vacuum chamber indicated in Figure 1. The pumping speed is regulated by a rotatable baseplate, which is also shown in Figure 1. The gas flows are regulated by needle valves and measured by calibrated mass flow meters. The partial pressures of the reagent in the interaction zone are calculated from the total pressures and from the reagent flows. For some experiments, a different reactor inlet is used, where only one reactant is irradiated by the laser. This reactor is described in a separate section below.

Room-temperature kinetic measurements of the rate constant for the $C_2H + SO_2$ reaction are performed with a different apparatus that has been described previously, and only a brief overview will be presented here.[37] A mixture of gases is continuously flowed into a vacuum chamber, which is pumped by a Roots blower (1000 L/s) backed by a mechanical pump (pumping speed ~60 L/s). The gas admitted into the chamber is mainly nitrogen, with small amounts of acetylene, oxygen, and SO_2 reactant. The background pressure is adjusted using a gate valve. After flows of the gases are established, an initial concentration of the C_2H radical is produced by 193 nm photolysis of acetylene using an excimer laser. Typical photolysis fluences inside the vacuum chamber are less than 10 mJ/cm^2 in an approximately 10 ns pulse. This minimizes the possibility of radical−radical reactions, such as $C_2H + O$. The decay of the C_2H concentration due to chemical reactions is monitored using the chemiluminescence tracer method, by adding oxygen to the gas flow. In this method, the concentration of C_2H is followed in time by observing $CH(A^2\Delta) \rightarrow CH(X^2\Pi)$ chemiluminescence produced by the $C_2H + O_2$ reaction. The chemiluminescence signal is detected using a photomultiplier tube with a 430 nm band-pass filter (10 nm band-pass) and recorded using a multichannel scaler in a photon counting regime. Typically, a radical decay profile is obtained by accumulating the signal from 6000 photolysis laser pulses. Time delays for the pulsing of the excimer laser and the multichannel scaler trigger are generated using a multiple channel digital delay generator. The experiment is run at a 10 Hz repetition rate. The concentrations of the reactants are calculated from the total gas density in the chamber ($3-6 \times 10^{16}$ molecule/cm^3) and the flow rates of the carrier gas, acetylene, oxygen, and the reactant SO_2, which are monitored using calibrated flow meters. The flow meters are calibrated by measuring a rate of pressure rise in a known volume.

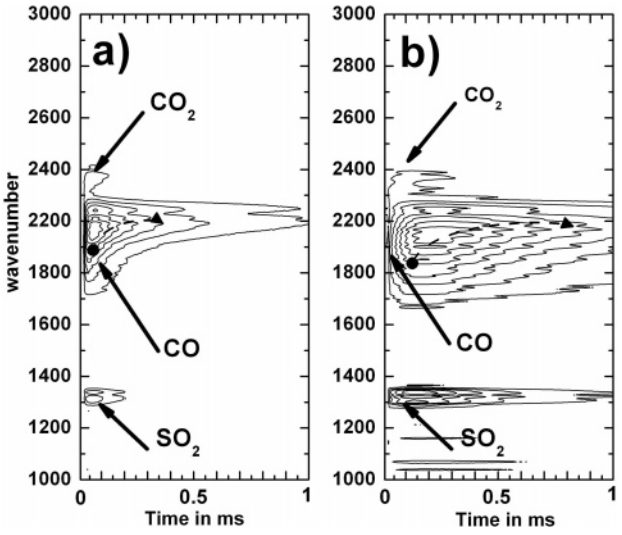

Figure 2. (part a) Time-resolved IR emission spectra of the $C_2H + O(^3P)$ reaction process with initial reagent pressures of $p(SO_2) = 43$ mTorr (6 Pa) and $p(C_2H_2) = 136$ mTorr (18 Pa). (part b) Same as part a with initial reagent pressures of $p(SO_2) = 126$ mTorr (17 Pa) and $p(C_2H_2) = 11$ mTorr (1.5 Pa). The total pressure is 1600 mTorr (213 Pa) with the balance due to Ar in the detection volume of the instrument. The observed products are CO, SO_2, and CO_2, indicated on the figure along with the vibrational deactivation of the excited CO product (dashed line).

Results

Infrared Spectra of the Products and Their Temporal Evolution. The temporal evolution of several low-resolution spectra taken at different initial reagent concentrations of C_2H_2 and SO_2 are shown in Figure 2a,b. These spectra are taken at 8-cm^{-1} spectral resolution and 5 μs temporal resolution using the mercury cadmium telluride (MCT) detector. There are two distinct features present in the spectra. The most intense feature is the CO emission ($v = 1 \rightarrow 0$ at 2143 cm^{-1}). Another strong emission is assigned to the vibrationally excited antisymmetric stretching mode of SO_2 (1362 cm^{-1}). This latter feature is present without added C_2H_2, indicating that this emission peak is probably due to the recombination of $SO + O$ and subsequent energy relaxation or to energy transfer (e.g., from vibrationally excited SO to SO_2). At the blue edge of the CO spectrum, some CO_2 emission is observed at significantly lower intensities than the CO band. The CO peak shifts to the red at longer times, which is an indication of vibrational relaxation. The vibrational deactivation varies between 100 and 200 μs at higher pressures (1600 mTorr, 213 Pa) indicated by dashed arrows in Figure 2a,b. The length of the reaction time is determined by three factors: consumption of the initial reagents, deactivation of the vibrationally excited products, and product fly out from the observation zone. Calculated from the flow velocities, the residence time of the products in the observation zone in Figure 2a is about 2.1 times shorter than in Figure 2b, which agrees well with the observed residence times.

In comparison of spectra at low total pressure (225 mTorr, 30 Pa) and high (1600 mTorr, 213 Pa) pressure (Figure 3), the low-resolution spectra at low pressure reveal three additional features that are missing from the high-pressure data. First, a

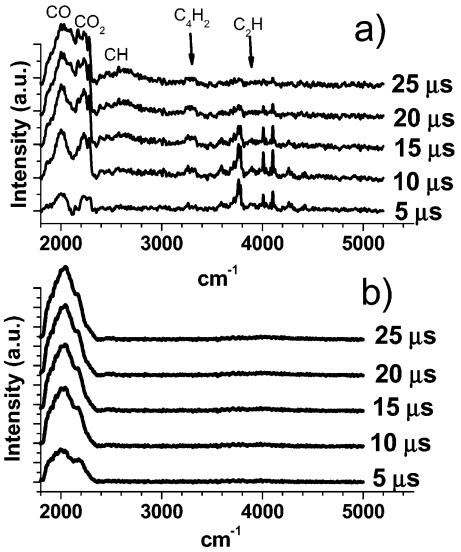

Figure 3. (part a) Time-resolved spectrum of $C_2H + O(^3P)$ reaction from 1800 to 5000 cm^{-1} at low-pressure $p_{total} = 225$ mTorr (30 Pa) total pressure. The data are taken with 8 cm^{-1} spectral and 5 μs time resolution using the InSb detector. (part b) Same as part a except $p_{total} = 1600$ mTorr (213 Pa) total pressure, resulting in a faster rate of deactivation.

prominent feature is initial emission from the C_2H radical in the 3500−4200 cm^{-1} wavelength range. This feature is mainly due to the emission from vibrationally excited states of the ground electronic state of C_2H, as well as the emission from the lowest excited electronic state of the $C_2H(\tilde{A}^2\Pi)$ radical.[30,31,38] As the total pressure increases, this feature disappears from the spectrum, suggesting efficient quenching of $C_2H(\tilde{A}^2\Pi)$ to its ground electronic and vibrational state. Another feature appears as a peak near 3300 cm^{-1}. This peak is present without the addition of SO_2 to the reaction mixture and is assigned to the vibrationally excited C_4H_2 hydrocarbon as a result of the $C_2H + C_2H_2$ reaction. The last feature is a broad emission in the 2400−2900 cm^{-1} range. This is tentatively identified as emission from CH. The signal in this wavelength range is very weak, and attempts to obtain high-resolution data were not successful even with several thousands of coadditions.

It is worthwhile to note that the spectra in Figure 2a,b reach their maximum intensities at very different times, which is the result of several factors. First, in Figure 2a, the reagent flow confined by the buffer gas into the observation zone is higher; therefore, the reagents and products are moving faster out of the observation zone. Second, the pressure of the acetylene is much greater in Figure 2a, and the acetylene is known to be an efficient quencher of vibrationally and electronically excited products.[26] Third, the depletion of either the $O(^3P)$ or C_2H concentration stops the reaction, resulting in the falloff behavior observed in Figure 2. The calculated flow velocity changes indicate that the first reason is the dominating factor in these experiments.

Obtaining the nascent vibrational distribution of reaction products requires separating the electronic, rotational, and vibrational relaxation times by appropriate choices of pressures and measurement times. Vibrationally and electronically excited radicals may react faster and can result in different products than radicals in the ground state. To ensure that the contribution of vibrationally and electronically excited C_2H and O radicals to the overall kinetics is small, the effect of the total pressure in the reaction system has been investigated. Low-pressure data indicate a variety of reaction products, which are important from the viewpoint of the reaction mechanism; however, to determine the nascent vibrational distribution of the reaction products, it is important that the observed product, such as CO, is not a result of reactions of electronically and vibrationally excited precursors. For this reason, the data for further studies in this paper are taken at high enough Ar total pressures to ensure the electronic and vibrational relaxation of C_2H radicals, but low enough to minimize the rate of vibrational relaxation of the

TABLE 1: Primary and Secondary Reactions in the $C_2H_2/C_2H/SO_2/SO/O$ Reaction System to Determine Contributions to the $C_2H + O$ Reaction[a]

		k_{298K} (cm^3/molecule·s)	ΔH^{298K} (kcal/mol)	included in the simulations
	Primary Reactions			
R1[24]	$C_2H(X^2\Sigma^+) + O(^3P) \rightarrow CO + CH(X^2\Pi)$	5.17×10^{-11}	−76.5	yes
R2[22−24]	$C_2H(X^2\Sigma^+) + O(^3P) \rightarrow CO + CH(A^2\Delta)$	4.5×10^{-12}	−10.5	yes
R3[62]	$C_2H(X^2\Sigma^+) + C_2H_2 \rightarrow C_4H_2 + H$	1.4×10^{-10}	−23.9	yes
R4	$C_2H(X^2\Sigma^+) + SO_2 \rightarrow$ Products	1.1×10^{-11}		yes
R5	$C_2H(X^2\Sigma^+) + SO_2 \rightarrow CO_2 + HCS$		−84.0	no
R6	$C_2H(X^2\Sigma^+) + SO_2 \rightarrow CO + SO + CH$		54.5	no
R7	$C_2H(X^2\Sigma^+) + SO_2 \rightarrow HCCO + SO$		103	no
R8	$C_2H(X^2\Sigma^+) + SO_2 \rightarrow CO + COS + H$		−80.9	no
R9	$C_2H(X^2\Sigma^+) + SO_2 \rightarrow COS + HCO$		−84.6	no
R10	$C_2H(X^2\Sigma^+) + SO \rightarrow CO + HCS$		−88.5	no
R11	$C_2H(X^2\Sigma^+) + SO \rightarrow HCCO + S$		−147.0	no
R12[63]	$C_2H_2 + O(^3P) \rightarrow CH_2(a^3B_1) + CO$	2.23×10^{-14}	−47	yes
R13[63]	$C_2H_2 + O(^3P) \rightarrow HCCO + H$	8.95×10^{-14}	−19	yes
R14	$C_2H_2 + SO \rightarrow HCCO + SH$		−101	no
R15	$C_2H_2 + SO \rightarrow CO + H_2CS$		−53.2	no
R16[64]	$SO + O(^3P) \rightarrow SO_2$	5.3×10^{-11}	−131.1	yes
	Secondary Reactions			
R17[25]	$CH(X^2\Pi) + O(^3P) \rightarrow CO + H$	1.0×10^{-10}	−175.1	yes
R18[18]	$CH(X^2\Pi) + C_2H_2 \rightarrow C_3H_{x(=1,2,3)} + H_{y(=3-x)}$	2.8×10^{-10}		yes
R19[65]	$CH(X^2\Pi) + SO_2 \rightarrow$ Products	3.08×10^{-10}		yes
R20[18]	$HCCO + O(^3P) \rightarrow 2CO + H$	1.6×10^{-10}	−101.8	yes
R21[18]	$HCCO + O(^3P) \rightarrow CO_2 + CH$	8×10^{-12}	−53.55	yes
R22[66]	$CH_2 + O(^3P) \rightarrow$ Products	1.34×10^{-10}		yes
R23[67]	$CH_2 + SO_2 \rightarrow$ Products	4.9×10^{-12}		yes
R25[68]	$CH_2 + C_2H_2 \rightarrow$ Products	2.99×10^{-12}		yes

[a] 1 kcal/mol = 4.2 kJ/mol.

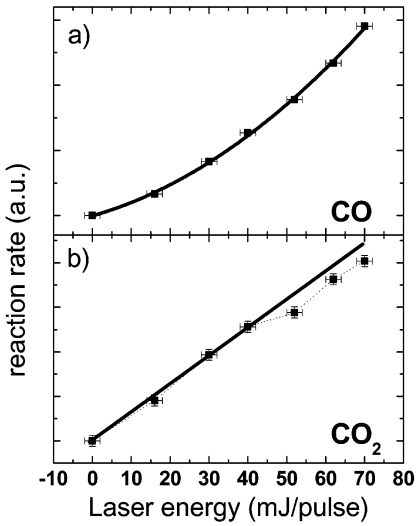

Figure 4. Power dependence of the CO (part a) and CO_2 (part b) signal at early times. The reaction rate has been determined by taking the CO signal at 5 μs with interference filters and plotting vs the laser power. The initial reagent pressures are $p(SO_2) = 126$ mTorr (17 Pa), $p(C_2H_2) = 11$ mTorr (1.5 Pa), and $p_{total} = 1600$ mTorr (213 Pa).

products.[39] The high total pressures ensure that the molecules suffer several collisions with the bath molecules before reaction, but at sufficiently short times that the vibrational relaxation of reaction products is minimal.

Power Dependence of the CO and CO_2 Signal. Table 1 shows the complete set of reactions that can occur in the photolysis of $C_2H_2 + SO_2$. There are many reactions that may result in the same products. The initial rate of formation of products from some of the reactions will exhibit a quadratic dependence on the photolysis energy, while for the other reactions, this dependence is expected to be linear. By measuring the initial product yields as a function of the photolysis energy, it may be possible to differentiate between reactions that produce the same vibrationally excited products based on the energy dependence. For the C_2H_2/SO_2 mixture, there are several reactions that all result in the same product, CO. The CO product from the $C_2H + O$ reaction is expected to show a quadratic dependence on the laser power. For the $O + C_2H_2 \rightarrow CO +$ products reaction, the laser power dependence is expected to be linear. Also, CO products may be formed through several secondary reactions, such as the $C_2H_2 + O$ reaction to produce HCCO, and its subsequent reaction, or the $CH + O$ reaction, where CH is a product of the $C_2H + O$ reaction. The greatest contributions from these other reactions can be determined. It is not obvious exactly how the products from the sequential reactions will depend on the laser power without doing kinetic simulations; however, it is expected that their dependence will be more than linear. Similarly, the CO_2 product may be produced in different reactions such as the $C_2H + SO_2$ and the $HCCO + O$ reactions. The former reaction is expected to show a linear dependence on the photolysis energy, as opposed to the latter.

The power dependencies of the CO and CO_2 signals have been investigated by collecting time-resolved signals using interference filters. The amplitudes of the signals taken at approximately 5 μs are plotted as a function of photolysis energy. For this time delay, the contribution from the secondary reactions is small, as has been checked by the kinetic simulations described later in the text.

The power dependence of the CO signal shows both linear and quadratic (Figure 4a) behavior. The quadratic behavior strongly suggests that the $C_2H + O$ reaction makes a contribution to the CO signal. The linear component is also very prominent, indicating that other reactions, such as $O + C_2H_2$, with a linear power dependence, contribute significantly. Figure 4b shows that CO_2 exhibits a nearly linear dependence on excitation power. The relatively low reagent concentrations ensure that only primary reactions contribute. On the basis of this assumption, the CO_2 product at early time is attributed to the $C_2H + SO_2$ reaction. The saturation of the CO_2 signal in Figure 4b is due to the decrease of the SO_2 concentration by photolysis, which becomes significant at about 60 mJ/pulse and not to a C_2H dissociation to form C_2, which takes place at higher laser fluences.

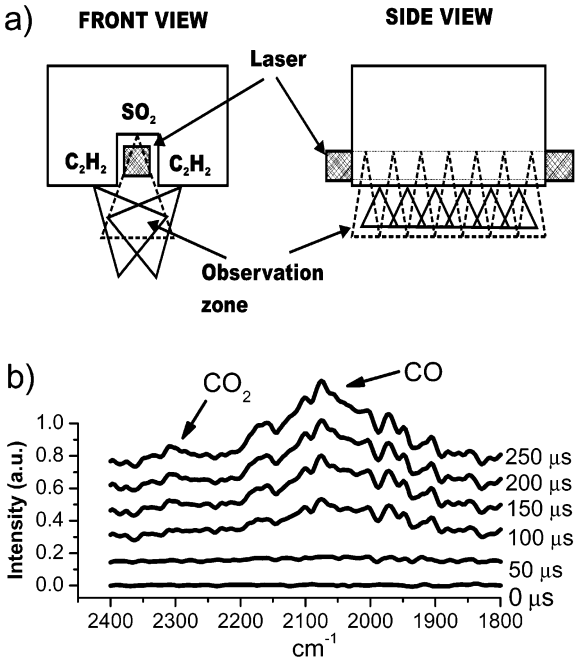

Figure 5. (part a) The simplified scheme of the reactor used in the experiment to determine the contribution of the $C_2H_2 + O$ and $C_2H + SO_2$ reactions. (part b) The observed time-resolved spectra of the reactions mentioned in part a. The initial reagent pressures are $p(SO_2) = 30$ mTorr (4 Pa) and $p(C_2H_2) = 30$ mTorr (4 Pa). The total pressure is 300 mTorr (40 Pa) with added Ar in the detection volume of the instrument.

Evaluating the $C_2H_2 + O$ and $HCCO + O$ Contributions. The dependence of the CO signal on the photolysis energy suggests that there is a noticeable contribution to the CO signal from reactions other than the $C_2H + O$ reaction. From Table 1, an obvious reaction to take into consideration is the $C_2H_2 + O$ reaction. To study this reaction, a different reactor is used, in which the radical (O), produced first by the photolysis, is subsequently mixed downstream with the reactant (C_2H_2).

The simplified scheme of the reactor is shown in Figure 5a. The reactor has two separate regions. The photodissociation of the precursor occurs in the center of the reactor. The radicals then flow into the interaction zone, where the actual reaction and observation take place. The reactant molecules are introduced into the system through small sets of holes located in parallel fashion at the center and the edges of the cell. The holes at the edges are aligned at a tilted angle to ensure better mixing of the reagents. The reactor replaces the effusive source described in the Experimental Section and is centered in the middle of the Welsh cell, parallel to the excitation laser beam.

For the study of the $C_2H_2 + O$ reaction, the SO_2 is introduced in the middle of the reactor, and the stream of photodissociated $SO_2 \rightarrow O + SO$ radicals is crossed with the stream of undissociated acetylene. As can be seen in Figure 5b, the C_2H_2

+ O reaction produces vibrationally excited CO and CO_2. The kinetics of the CO_2 formation and a strong quadratic laser power dependence observed with this separated reagent reactor indicate that CO_2 may be produced in a secondary reaction. This secondary reaction is discussed in detail in another publication[40] and is assumed to be the HCCO + O reaction, which occurs after formation of HCCO from the C_2H_2 + O reaction. The CO and CO_2 signals in Figure 5b are comparable in amplitude to the CO and CO_2 signals obtained with the effusive source in Figure 2. It is also observed that there is no dramatic difference in the CO and CO_2 signals when SO_2 and C_2H_2 are premixed or flowed separately through the center of the reactor in Figure 5a. It has to be emphasized that this reactor is not able to capture the early time behavior of the C_2H_2 + O reaction because of its inherent design, and so, direct comparison of the relative amount of CO from C_2H + O and C_2H_2 + O is not possible. These results suggest the following conclusions: (1) The observed CO subquadratic power dependence at early times is mainly due to the C_2H_2 + O reaction at early times. (2) In Figure 2, the observed CO has a contribution from the C_2H_2 + O and HCCO + O reactions. (3) The CO_2 product observed in the experiments using the effusive source is at least partially due to the HCCO + O reaction.

Evaluating the $C_2H + SO_2$ Contribution. The linear power dependence of the CO_2 emission at early times (Figure 4b) strongly implies (Table 1) that the $C_2H + SO_2$ reaction occurs in the typical reaction mixture. To verify this suggestion, two separate experiments are carried out. The total removal rate constant and the product emission from this reaction are measured using two different experimental setups, described in the previous sections. For the rate constants, the flow tube reactor is used.

Rate constants for the $C_2H + SO_2$ reaction are measured under pseudo-first-order conditions where the concentration of the SO_2 reagent is much larger than the C_2H concentration. The kinetics of C_2H removal under these conditions can be expressed as

$$\frac{d[C_2H]}{dt} = [C_2H](k_{SO_2}[SO_2] + k_{oxygen}[O_2] + k_{acetylene}[C_2H_2]) = k_{obs}[C_2H] \quad (1)$$

where k is the rate constant for the $C_2H + SO_2$ reaction. The bimolecular rate constant, k_{SO_2}, is determined by plotting the observed first-order decay rate constant, k_{obs}, versus the reagent concentration, $[SO_2]$.

Chemiluminescence from the electronically excited $CH(A^2\Delta)$ radical produced in the C_2H reaction with O_2 is used to follow the C_2H concentration in time. Details of the 193 nm photolysis of C_2H_2 to create an initial concentration of C_2H radical and the chemiluminescence tracer method are discussed previously.[24] Under the conditions of this experiment, the chemiluminescence signal is proportional to the C_2H concentration. A typical decay of the chemiluminescence signal is shown in Figure 6a. As can be seen, the plot of the natural logarithm of the signal versus time is linear, confirming that the experiment is done under pseudo-first-order conditions. First-order decay rate constants, k_{obs}'s, are determined from plots such as those shown in Figure 6a by linear least-squares fitting. Fitting is done starting at a 25 μs delay after the photolysis laser pulse to avoid interference from the scattered laser light and emission produced by the photolysis pulse. Figure 6b shows plots of the first order decay constants versus the SO_2 reactant concentration. The slope of the line gives the bimolecular rate constant, k_{SO_2}. The intercept

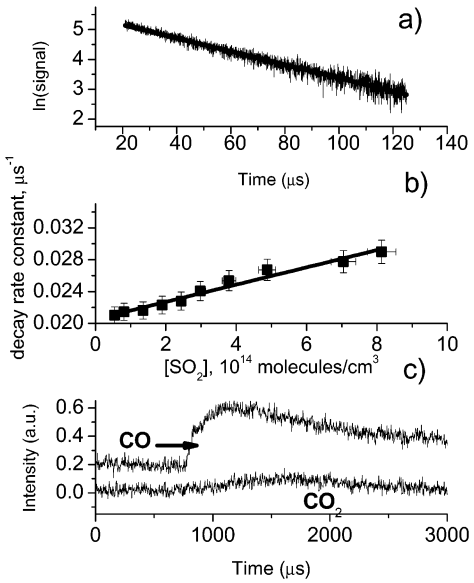

Figure 6. (part a) The natural log of the CH chemiluminescence used to trace the $C_2H + SO_2$ reaction. (part b) The decay rate constants of CH chemiluminescence vs SO_2 concentration. (part c) The IR CO and CO_2 signal from the $C_2H + SO_2$ reaction. The initial reagent pressures are $p(SO_2) = 30$ mTorr (4 Pa) and $p(CF_3CCH) = 30$ mTorr (4 Pa). The total pressure is 300 mTorr (40 Pa) with added Ar in the detection volume of the instrument.

of the first-order rate constant versus the reactant concentration plot is mainly due to C_2H reactions with acetylene and oxygen and, to a lesser extent, the diffusion of C_2H radicals out of the irradiated zone.

The rate constant is measured for two values of the total pressure, 1.0 Torr (133 Pa) and 2.05 Torr (273 Pa). Both measurements give essentially the same values for the rate constant, and the average rate constant is $(1.1 \pm 0.3) \times 10^{-11}$ cm^3 $molecule^{-1}$ s^{-1}. The indicated uncertainty (2σ) of the rate constants includes both the statistical (<5%) and systematic errors. Because the SO_2 molecule has a large absorption cross section at 193 nm, it is possible that the measurements of the rate constants may be affected by the reactions of C_2H with the fragments of SO_2 photolysis, which are O and SO. To test whether these possible interfering reactions play any role in the kinetic determinations, the rate constants are measured for significantly different values of the photolysis energy. Because the rate constant for the C_2H + O reaction[24] is approximately four times larger than the measured rate constant for the C_2H + SO_2 reaction, it is expected that an increase in the photolysis energy would produce an increase in the measured rate constant. Two measurements were done for photolysis energies that differ by a factor of five, and both measurements give the same result within the statistical uncertainty. A simple calculation is also done in which, from the dissociation fraction of SO_2, the contribution of the possible interfering reactions to the overall rate constant is estimated. Both the experimental test and the calculation confirm that the systematic error due to the interfering reactions can be neglected. This is possible because of the much lower photolysis laser energy density in the kinetic measurements compared to the FTIR experiments. In the FTIR experiments, both the $C_2H + SO_2$ and the C_2H + O reactions are important.

To determine whether the $C_2H + SO_2$ reaction contributes to the observed CO and CO_2 signal, the $C_2H + SO_2$ reaction is investigated using the same reactor described previously (Figure 5a). This time, the C_2H precursor is introduced through the middle set of holes in the reactor, and the SO_2 is introduced

through the outer part of the reactor, ensuring spatial separation and selective photodissociation of the C_2H precursor. In this experiment, instead of using C_2H_2 as a precursor for the C_2H radical, CF_3CCH is used as the precursor for C_2H for the following reasons. The absorption cross section of CF_3CCH at 193 nm is much larger than that of C_2H_2, which results in higher initial concentrations of C_2H. Also, the CF_3CCH reacts with C_2H more slowly compared to C_2H_2, which reduces losses of C_2H due to chemical reactions during the time it takes the C_2H radicals to reach the observation zone. Figure 6c shows the time development of the CO and CO_2 signals through the interference filters. Both signals persist for several milliseconds. There is a small spike at the rise of the CO signal, which is due to the reactor used in this experiment that partially blocks some of the signal as the reaction volume moves through the observation zone of the Welsh cell. The overall signal strength of the CO is about 10−15 times weaker than the overall signal strength when mixing the SO_2 and C_2H_2 and introducing the reactants through the same reactor inlets so that both O and C_2H are produced. Note that the photolysis yield for C_2H production from CF_3CCH should be larger than from C_2H_2. Also, the reactive loss of C_2H is significant in the photolysis of acetylene, while in CF_3CCH photolysis, the reaction of C_2H with CF_3CCH is much less. A previous study[41] suggests that the 193-nm photolysis of CF_3-CCH results in more C_2H radicals by approximately a factor of two. Despite these weaknesses in the comparison experiment, the results suggest that there is a contribution to the observed CO signal from the $C_2H + SO_2$ reaction; however, the contribution appears to be less significant than that from the $C_2H_2 + O$ reaction. The $C_2H + SO_2$ reaction has many possible products (Table 1), which may account for its relatively weak CO and CO_2 emissions. The results of the observable product distributions for the $C_2H + SO_2$ reaction will be investigated in the future. No further assessment of this reaction will be considered in this study, but the $C_2H + SO_2$ reaction is included in the simulations below, by way of an upper limit contribution.

Kinetic Modeling. To understand the kinetics of the C_2H_2/SO_2 system and to see under what conditions the $C_2H + O(^3P)$ reaction can be separated from the other reactions, a kinetic simulation is done. Table 1 summarizes the important reactions that could be identified from the literature and the preliminary results obtained here. It should be noted that the reaction of $CH + O(^3P)$ is a factor of two faster than $C_2H + O(^3P)$, making it a possible secondary reaction that produces CO. The exothermicity of $CH + O(^3P)$ is much larger than that of $C_2H + O(^3P)$, resulting in a different vibrational distribution for CO. Thus, it is desirable to have C_2H in excess of O to minimize the secondary process. However, this could not be achieved. The absorption cross-section of acetylene[26,33] at 193 nm is approximately 60 times less than the absorption cross-section of SO_2.[42,43] Also, the removal of the C_2H radical is very efficient by several processes such as the $C_2H + C_2H_2$ reaction. These two problems could be circumvented by using the CF_3CCH precursor, but this precursor is available only in small quantities. In addition to the fast CH + O reaction, which will be discussed, $O(^3P)$ can react with C_2H_2 to produce some CO, as well as HCCO, which subsequently reacts with O to produce CO and CO_2. Each of these paths is addressed by the model in order to determine the conditions suitable to extract the nascent vibrational distribution of the $C_2H + O(^3P)$ reaction.

The time evolution of the concentrations of the various species can be solved numerically by evaluating a set of coupled differential equations or by using a stochastic method.[44−46] In a stochastic method, the time history of a chemical system is calculated on the basis of the reaction probabilities using the reaction's mechanism and the specified initial conditions. In the present study, the stochastic method is used to predict the time evolution of the reaction system. The rate constants used in the simulation are given in Table 1. The initial concentrations of C_2H and $O(^3P)$ are determined by the absorption cross-sections of acetylene (1.39×10^{-19} cm^2/molecule)[26,33] and SO_2 (6×10^{-18} cm^2/molecule)[42,43] and the quantum yields of 193-nm photolysis. The C_2H quantum yield from 193-nm photolysis of C_2H_2 has a wide range of values,[26,33,47] but in this paper, the most recent value (0.94) is used.[26,33] The quantum yield for $O(^3P)$ production is taken to be unity. The energy of the laser beam in the excitation volume is approximately 60 mJ/pulse for a 5 mm × 12 mm beam size. It should be noted that the determination of absolute number densities is difficult, because the exact pressure is approximated with the pressure that is measured on the side of a large chamber. The actual pressure is slightly larger. Also, the observed kinetics may show slower rise times due to the density gradient and fly-out of the products from the observation zone. These two effects may approximately cancel each other. In addition, the observed signals are not directly related to the concentrations of products, because they have very different vibrational excitations.

In the simulation, especially for the CO(v) product, a few assumptions are made, which are as follows: (a) the included reactions are sufficient to appropriately describe this reaction system, (b) the rate constant for R1 is calculated from the well-determined rate constant of R1 + R2 and its previously reported branching ratio (92%), (c) the rate constant for R8 is equal to that for R4. Because the $C_2H + SO_2$ total rate constant is measured, it allows an estimate of the upper limits for the CO and CO_2 channels in this system. (d) SO does not react with C_2H_2 or C_2H at room temperatures, or its rate constants for CO production are not comparable to the rate constants of the $C_2H_2 + O$ and $C_2H + O$ reactions. This assumption is based on the following analogy: If we assume that C_2H with SO is as reactive as or less reactive than C_2H with the isolectronic O_2 molecule, then the reaction rate constant for CO production by $C_2H + SO$ is expected to be an order of magnitude smaller than $C_2H + O$. The room-temperature rate constant of $C_2H + O_2$ is 3.2×10^{-11} cm^3 molecule^{-1} s^{-1},[48] which is comparable to R1; however, the CO channel is only a small fraction (12%) of the total rate.[49] Also, the highly exothermic reactions of $C_2H + SO$ (R10 and R11) should produce other vibrationally excited photoproducts (HCCO and HCS), which are not observed in our experimental conditions.

Figure 7 shows that there are several different reactions that produce CO in this system; however, at early times, the CO signal is dominated by R1 (F in Figure 7) and R8 (E in Figure 7). The CH + O (A in Figure 7) reaction, surprisingly, is of relatively little importance in the first few tens of microseconds, because CH reacts rapidly with C_2H_2. C and D correspond to R12 ($O + C_2H_2$) and R20 (HCCO + O), respectively, which have intermediate importance at early times but dominate the CO signal at longer times. This is expected, because the initial radical concentrations are relatively small, so even reactions with a small rate constant, but large reagent concentrations (C_2H_2 and SO_2, O are in excess), could make significant contributions to the observed CO signals at later time.

As the data show, several reactions contribute to the CO signal, and it is difficult to quantify all the different channels and their contributions. However, only one component of these CO contributions at early times should have a quadratic laser power dependence ($C_2H + O$). The quadratic part of the CO

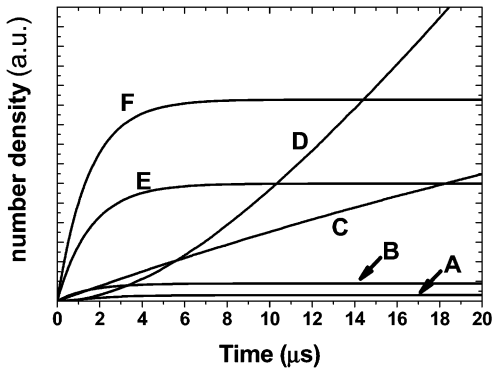

Figure 7. The first 20 microseconds of the simulated time evolution of the CO signals broken down into individual reactions, with initial reagent pressures of $p(SO_2) = 126$ mTorr (17 Pa) and $p(C_2H_2) = 11$ mTorr (1.5 Pa). The laser energy is assumed to be 60 mJ/cm^2. Labels (see Table 1): A, R17; B, R2; C, R12; D, R20; E, R8; F, R1. Because the reagent pressures may not be accurately measured in the interaction region, the time scales of the simulations may not agree with the experimental observations.

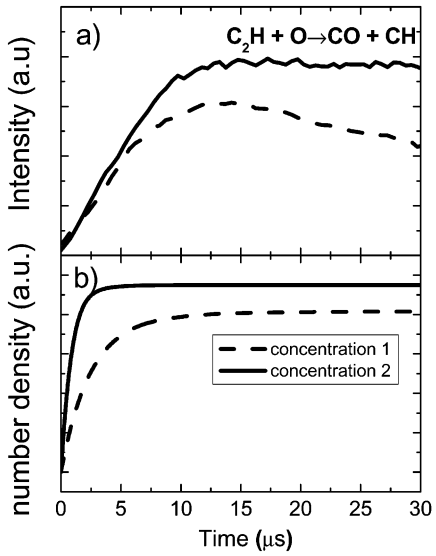

Figure 8. (part a) The filter kinetics data of the $C_2H + O$ reaction. The data are taken at 60 mJ/pulse laser power, and a trace of low laser power data at 16 mJ/pulse is subtracted. Both data are normalized before subtraction, and the initial reagent pressures for concentration 1 and concentration 2 are $p(SO_2) = 126$ mTorr (17 Pa) and $p(C_2H_2) = 11$ mTorr (1.5 Pa)and $p(SO_2) = 43$ mTorr (6 Pa) and $p(C_2H_2) = 136$ mTorr (18 Pa), respectively. The total pressure is 1600 mTorr (213 Pa) with added Ar in the detection volume of the instrument. (part b) The corresponding simulation to the data in Figure 8a.

signal can be extracted from the signal by subtracting a signal taken at low power, where the reaction is dominated by the radical + precursor molecule reactions. To achieve this goal, an appropriate normalization for the linear part is required, which is done by dividing the observed CO signal by the excitation power. A similar procedure is used to acquire the spectra to determine the nascent $C_2H + O \rightarrow CO(v) + CH$ vibrational distribution, thus eliminating the possible $C_2H + SO_2$ contribution. Figure 8a shows the observed CO emission from the $C_2H + O$ reaction at two different concentrations after this normalization, collected using an interference filter and after subtracting the low-power data. The corresponding simulation without vibrational deactivation and fly out is shown in Figure 8b. For the simulation results, the calculated low-power data are also subtracted to give a direct comparison between the experiment and the simulation. The qualitative time scales of the data and

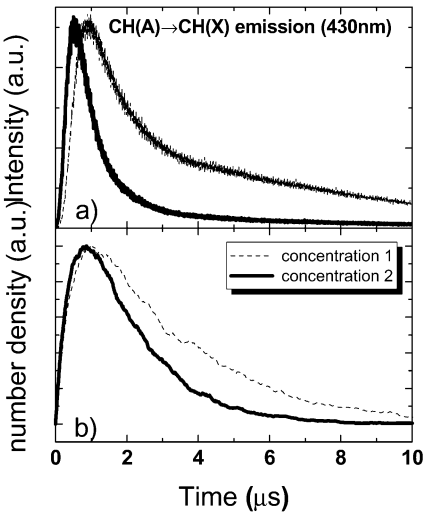

Figure 9. The 430-nm emission of the $CH(A^2\Delta)$ at two different concentrations. The emission is collected with a photomultiplier tube and interference filter. (part a) The initial reagent pressures for concentration 1 and concentration 2 are $p(SO_2) = 126$ mTorr (17 Pa) and $p(C_2H_2) = 11$ mTorr (1.5 Pa) and $p(SO_2) = 43$ mTorr (6 Pa) and $p(C_2H_2) = 136$ mTorr (18 Pa), respectively. The total pressure is 1600 mTorr (213 Pa) with added Ar in the detection volume of the instrument. (part b) Simulation corresponding to the data in part a.

the ratio of the CO production for the two different concentrations agree with the simulations. However, the simulations in Figures 7 and 8b predict more rapid rise times than observed experimentally in Figure 8a. The difference in time scales may be due to several factors. It is assumed that the linear power-dependent part of the CO signal is a pseudo-first-order reaction, which is a rough estimate, because the concentration of O is only three times less than the concentration of SO_2. The actual signals can involve cascades of vibrational deactivation. The biggest issue is that the estimates of the densities in the interaction region may differ from the values used in the simulation because of the significant gas density gradients emanating from the source.

In separate experiments, the time scale for the $C_2H + O$ process can be determined by monitoring the CH radical species, which has to come from this reaction. The excited CH radical is a direct result of the $C_2H + O$ reaction and can be detected by its 430 nm emission, similar to the kinetics experiment described in the earlier section. The radiative lifetime of the $CH(A^2\Delta)$ is relatively short (470 ns), which makes it a very attractive probe. The results set the desired time scale for analysis of the $CO(v)$ spectra. The observed time-resolved CH emission is shown in Figure 9a at two different concentrations. The corresponding simulation is also shown in Figure 9b. In the simulation, the emission lifetime of the $CH(A^2\Delta)$ state is also taken into account. A decrease in the C_2H_2 concentration (decrease in the C_2H concentration as well) results in a longer reaction time. The slower rise of the CH signal is due to the change in the [O] concentration, which determines the rise time in the pseudo-first-order regime ($[O] \gg [C_2H]$). This is in agreement with the simulation. The simulation predicts a little slower rise and decay, which might be because not all of the radical quenching processes are included in the simulation and the estimated concentrations in the interaction region are not exact. The conclusion is that the radical−radical reaction proceeds very rapidly and is finished in the first few microseconds. The simulation suggests that the main reason that the radical−radical reaction stops is the removal of the C_2H radical from the reaction system.

Nascent Vibrational Distribution of the $C_2H + O(^3P)$ Reaction. The nascent vibrational distribution of CO from the $C_2H + O$ reaction is obtained by collecting high-resolution spectra in an argon buffer. The initial concentrations are $p(SO_2) = 43$ mTorr (6 Pa) and $p(C_2H_2) = 136$ mTorr (18 Pa). The total pressure was 1600 mTorr (213 Pa) with added Ar buffer. During the collection, an interference filter is used to increase the sensitivity of the detection. For one spectrum, 100 coadditions are used to evaluate the nascent vibrational spectra of CO. The spectral resolution is measured to be 0.37 cm^{-1}, which is calculated from individual CO lines. The resulting spectrum is normalized for the instrument response function of the detection. The instrument response function is determined by measuring the spectrum of an ideal blackbody source at 950 K with the same filter used in this experiment. As we concluded in the previous section, the best condition to obtain the nascent vibrational distribution of the $C_2H + O$ reaction is at early time. Thus, the fast external digitizer card is used to obtain data at 500-ns time resolution. To obtain the nascent vibrational distribution of the $C_2H + O$ reaction, the data are taken at low (9 mJ/pulse) and high power (60 mJ/pulse) under identical circumstances. The data are normalized to the power and from the high power data the low power data are subtracted. The nascent CO(v) vibrational distribution of the $C_2H + O$ reaction is measured at 10 μs for several reasons. It is desirable to minimize the contribution to the total signal from electronically or vibrationally excited precursors, and at earlier times, these are more likely to contribute a larger fraction of the total signal. At times earlier than 10 μs, the total signal from the desired reaction is much less so it is advantageous to take data when the number density of the vibrationally excited CO molecules is at a maximum (see Figure 8). At later times, there are several other contributions to consider. These are the vibrational deactivation of the CO and secondary reactions from $CH + O$ and $HCCO + O$, which can also exhibit a quadratic dependence on the excitation power. The vibrational deactivation is on the order of a few hundred microseconds (see Figure 2), which is not a significant problem for data taken at 10 μs. The relative concentration of C_2H_2 is increased in comparison to the simulations, in order to allow data to be obtained at later times without interference from the $HCCO + O$ reaction. Low-resolution data taken using the same conditions described above indicate that, upon subtraction of the laser-power-normalized low-power spectrum from the laser-power-normalized high-power spectrum, the CO_2 peak completely disappears, which can only happen if the $HCCO + O$ reaction is not a significant contribution at 10 μs. The same conclusion can be reached on the basis of the power-dependent emission data through selected interference filters in Figure 4b.

The extraction of the nascent vibrational distribution is based on spectroscopic simulation and fitting of the experimental spectrum. First, the simulation calculates the spectral positions of CO from the well-known spectroscopic constants.[50] The stick spectrum is calculated from the rotational and vibrational populations and then normalized by the Einstein A coefficients[51,52] for the vibrational transitions. At each vibrational transition, a Boltzmann rotational population is used with a corresponding rotational temperature. The rotational relaxation occurs rapidly,[53] so using a Boltzmann-like distribution is justified under the present conditions. The stick spectrum is convolved with the instrument response function to account for the finite resolution of the instrument. The simulation program allows varying the vibrational populations, the rotational temperature of each vibrational transition (typically 300 ± 50 K),

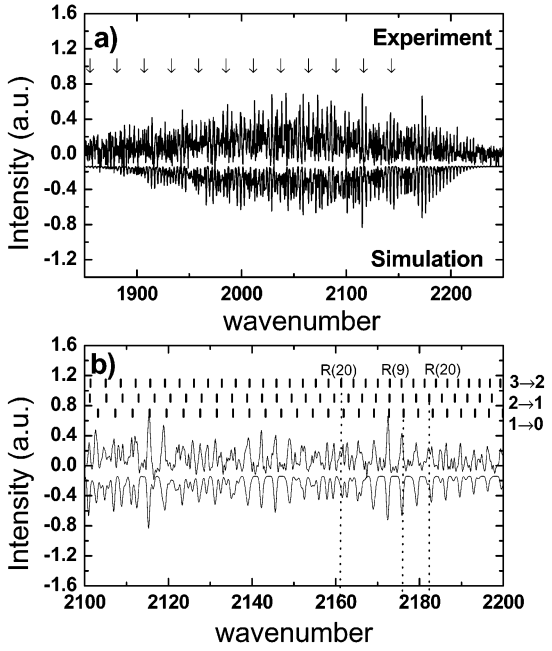

Figure 10. (part a) The full experimental (upper) and simulated (lower inverted) spectrum of vibrationally excited CO from the $C_2H + O(^3P)$ reaction. The arrows indicate the centers of vibrational transitions from $v = 1$ to $v = 12$ (right to left). (part b) A small section of the full experimental and simulated spectrum from 2150 to 2220 cm^{-1}. The positions of the first three vibrational transitions are indicated at the top of the graph with a series of vertical lines. The dashed line indicates a particular rotational transition for each vibrational transition.

and the instrument resolution of the spectrometer. The error function of the simulation compared to the experimental spectra is minimized to obtain the vibrational populations. The instrument resolution is sufficient to resolve some rotational lines (0.37 cm^{-1}), but at higher v's, not all rotational lines are well separated. However, fitting the overall spectrum allows accurate determination of the vibrational populations. A portion of the simulated data and the experimental data for the CO emission is presented in Figure 10. The lower graph shows the inverted simulated spectrum and the upper part shows the experimental data along with the first three assigned rovibrational transitions. The spectrum could be fitted up to $v = 12$ only, but the exothermicity of the $C_2H + O(^3P)$ reaction would allow up to $v = 14$ (including the anharmonicity of the CO vibration). This difference is mainly due to the fact that the spectral sensitivity of the InSb detector drops significantly at approximately 1800 cm^{-1} (The centers of the $v = 13$ and 14 vibrational transitions are located at 1830 and 1804 cm^{-1}, respectively).

Analysis of the CO Nascent Vibrational Product Distribution of the $C_2H + O(^3P)$ Reaction. Figure 11a shows the nascent vibrational distribution of the vibrationally excited CO product obtained by the fit from the data in Figure 10. For interested readers, the vibrational distributions from $v = 1$ up to $v = 12$ are 0.407 ± 0.005, 0.171 ± 0.01, 0.089 ± 0.01, 0.058 ± 0.01, 0.043 ± 0.02, 0.047 ± 0.02, 0.05 ± 0.02, 0.047 ± 0.03, $0.027 + 0.03 - 0.027$, $0.019 + 0.03 - 0.019$, $0.027 + 0.03 - 0.027$, and $0.012 + 0.03 - 0.012$. The error bars are determined from the changes in the error function for the fit as the population at each level is changed. The nascent vibrational distribution of the $C_2H + O$ reaction is expected to result in two different CO distributions depending on whether the reaction yields the $CH(A^2\Delta)$ or $CH(X^2\Pi)$ state. It is possible to obtain a bimodal distribution from a single reaction resulting in the same products; however on the basis of previous observations[22,23] of the occurrence of the $CH(A^2\Delta)$ channel, this

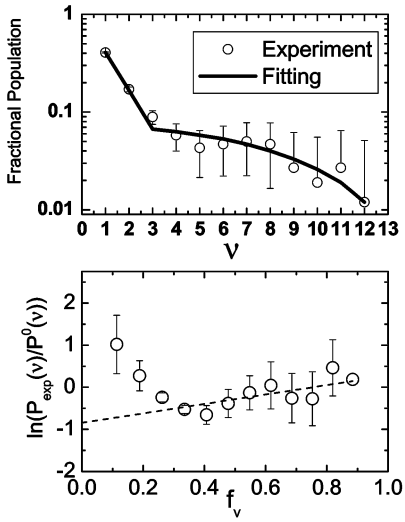

Figure 11. (part a) Experimentally determined nascent distribution of CO(v) from the $C_2H + O$ reaction along with the surprisal fit. (part b) The surprisal plot of the $C_2H + O$ reaction as a function of f_v for the CH($X^2\Pi$) channel. This plot demonstrates that the linear surprisal is valid for the CH($X^2\Pi$) channel. The actual values of the λ parameters are extracted from a simultaneous fit (see text).

possibility is dismissed. The exothermicities of these two reactions are vastly different, as shown in Table 1. The available energies for both reactions can be calculated from the exothermicities, the activation energies of these reactions, and the thermal energies of reactants. The available energies are 28 330 and 5113 cm^{-1} for R1 and R2, respectively. These values correspond to maximum levels $v = 14$ and $v = 2$, CO vibrational quantum numbers, respectively, that can be populated in these two reactions, including the anharmonicity corrections for the vibrational energy levels. Figure 11 shows that the vibrational distribution is dominated by R1 at high v, but it also consists of significant R1 at low v. The energy disposal of a chemical reaction can be characterized by the surprisal parameters, which are a measure of the deviation of the measured vibrational, translational, or rotational energy release from the calculated prior distribution, predicted on the basis of the maximum entropy postulate.[54] To obtain the surprisal parameters and the branching ratio of R1 and R2, the nascent vibrational distribution of the CO is fitted with a linear combination of two surprisals

$$P_{\text{Total}} = fP_1(\lambda_1) + (1 - f)P_2(\lambda_2) \tag{2}$$

The fitting function contains three parameters. Each surprisal is assumed to be linear, and the deviation from the statistical distributions is characterized by two λ parameters. The relative contribution of each reaction is characterized by the fraction (f). The prior vibrational distribution ($P^0(v|E)$) of this reaction is calculated using the following formulas

$$P^0(v|E) \propto \frac{(1 - f_v)^{3/2}}{\sum_{v=0}^{\max}(1 - f_v)^{3/2}}$$

$$f_v = \frac{E_v}{E}$$

$$E_v \le E \tag{3}$$

Here, f_v corresponds to the ratio of the vibrational energy (E_v) to the total available energy (E). The best fit is shown in Figure 11a along with the experimental data. The surprisal plot considers the $\ln(P/P^0)$ as a function of f_v for a single reaction channel. The construction of the surprisal plot for the CH(X) channel is shown in Figure 11b. From this plot, the λ_1 parameter can be extracted. A separate plot obtains the λ_2 for the CH($A^2\Delta$) channel by first subtracting the distribution for the CH($X^2\Pi$) channel. It can be seen that the data can be fit with two straight lines. The data points at higher f_v values correspond to the CH($X^2\Pi$) channel and at lower f_v values correspond to the CH($A^2\Delta$) channel. It should be noted that the CH($A^2\Delta$) channel is not a function of f_v for CH($X^2\Pi$), which would result in a large negative slope (positive λ in Figure 11b). This plot only demonstrates the construction of simultaneous linear surprisals, not the actual extraction of the λ's. In the actual fitting process, the data in Figure 11a are fitted with eq 2, which naturally would not result in a linear plot as a function of vibrational populations. The surprisal parameters for R1 and R2 are -1.5 ± 0.2 and -1.1 ± 0.2, respectively, showing only a small deviation from the statistical distribution. The f is found to be 0.4 ± 0.2 for R1, meaning that 40% of the $C_2H + O$ reaction proceeds through R1. This number includes the extrapolation of the measured vibrational distribution to the vibrational ground state. The negative λ values indicate preferential disposal of the reaction energy to the vibrations of the CO product.

Discussion

Several vibrationally excited products of the $C_2H + O(^3P)$ reaction are observed, which are CO, CO_2, SO_2, C_4H_2, CH, and SO_2. The major product of the reaction mixture is CO. Some of the products, such as CH and C_4H_2, can only be observed at low buffer gas pressures (Figure 3) because of the lesser extent of vibrational and chemical quenching processes at these pressures. The much lower Ar pressure reduces the confinement effect and decreases the absolute number densities quickly. The SO_2 peak at 1389 cm^{-1} in Figure 2 corresponds to the ν_3 antisymmetric stretching mode of SO_2, which is the result of recombination of SO with $O(^3P)$, which has been previously studied by TR-FTIR.[55] The rise of SO_2 emission is an efficient indicator of the presence of O atoms in the reaction system. CH radical vibrational emission could be observed only at lower pressures and only with low spectral resolution (with interference filters).

Besides the desired $C_2H + O$ reaction, several other primary reactions can contribute to the observed vibrationally excited products. Two major ones are identified as the $C_2H_2 + O$ and the $C_2H + SO_2$ reactions. The $C_2H_2 + O$ reaction is a prominent one in this system and is the major reaction responsible for the strong linearity of the power dependence of the CO signal. The $C_2H_2 + O$ reaction primarily results in CH_2, CO, and HCCO products. The HCCO also reacts subsequently with O, resulting in additional vibrationally excited CO, which has a strong nonlinear dependence similar to the $C_2H + O$ reaction; however, it should be pointed out that this reaction occurs on longer time scales (several hundred microseconds). The same argument is true for the CH_2 (from R12) + O reaction. The importance of this reaction is much less because of a much smaller branching ratio for CH_2 to be formed by R12.

The rate constant for the $C_2H + SO_2$ reaction, determined in this work, is $(1.1 \pm 0.3) \times 10^{-11}$ cm^3 $molecule^{-1}$ s^{-1}. This rate constant is an order of magnitude less than the CH + SO_2 reaction, which is consistent with the lower reactivity of the C_2H radical compared to the CH radical. There are several

products observed that are associated with this reaction. The best indicator of this reaction is the prompt CO in the system (See Figure 6c). In Figure 4b, the power dependence of the CO_2 signal at early times is linear, suggesting that the relatively prompt CO_2 is due to the $C_2H + SO_2$ reaction, which is different from the CO_2 from the HCCO + O reaction. The latter is a secondary reaction, and its appearance is expected to be sigmoidal. In addition, the power dependence of the CO_2 from the HCCO + O reaction would show quadratic behavior. The reaction is also investigated by the separated reactor design allowing an independent study of this reaction with interference filters, which confirms that the $C_2H + SO_2$ reaction may proceed by at least two channels resulting in CO and CO_2.

There are other electronically or vibrationally excited precursors that could contribute to the signals in this reaction system, such as C_2H^*, vinylidine, SO_2^*, SO^*, C_2^*. The 193 nm photolysis of acetylene is known to produce a mixture of vibrationally and electronically excited C_2H.[30,31,38] After photolysis, the average available energy for C_2H is 5530 cm^{-1}.[56] The 193-nm photolysis of C_2H_2 results in about 50% $C_2H(\tilde{X})$ and 50% electronically excited $C_2H(\hat{A})$ and a minor amount of $C_2H(\tilde{B})$. The C_2H radical has the low-lying electronic state ($C_2H(\hat{A})$) along with several vibrational modes that make it relatively easy to detect in the IR region. At lower total pressures (~200 mTorr, 27 Pa) and using similar concentrations of the reaction precursors as in the higher total pressure measurements, the lifetime of the vibrationally and electronically excited C_2H is long enough that it can be easily detected (Figure 3). The lower pressures also affect the fly-out time and decrease the absolute concentrations, which facilitate the observation of intermediate species in the reaction system. Also, the lower relative buffer gas concentration reduces the electronic and vibrational relaxation rates. Under the experimental conditions used to determine the nascent vibrational distribution of CO, the C_2H radical did not exhibit any emission, indicating that the C_2H radical was relaxed quickly to its electronic and vibrational ground state. The relaxation is facilitated by molecular collisions with buffer molecules. The electronic quenching and vibrational deactivation of the initial reagents is addressed by studying the effect of the total pressures and the type of buffer gas used in the experiments. Ar and N_2 are known to have vastly different quenching rates for the $C_2H(\tilde{A}) + M \rightarrow C_2H(\tilde{X})$ process,[26] but no noticeable difference could be observed on the CO kinetics at early times for these different types of buffer gases at the highest pressures used in the spectral experiments. The importance of the vibrational deactivation and electronic quenching of the reagent molecules is best demonstrated in Figure 3, where at low pressures, the vibrationally and electronically excited C_2H radical emission can be observed along with several other products that are not observable at higher pressures. On the basis of simple considerations of the detectivity in the experimental setup and the number density of the molecules in the observation zone, and assuming some initial concentrations (50% electronically and vibrationally excited C_2H), 99% of the C_2H radicals are in their ground electronic and vibrational state after a 1 μs, whereas the typical rise time of the CO(v) signal under the same condition is 6−7 μs.

Comparison of the high-pressure and low-pressure ratios of the CO and CO_2 signals is very different, indicating that the reactivity of some of the unrelaxed initial radicals may be very different compared to the reactivity of their relaxed counterparts. It is also possible to address the effect of total pressure on the nascent vibrational, rotational distribution of the CO product. The pressures used in the experiment are high enough that even at early times the rotational population reaches an equilibrium, and the vibrational relaxation at these pressures takes approximately tens of microseconds. The conclusion is that at higher total pressures the vibrational deactivation and electronic quenching are faster than the reaction rates observed.

To simulate the reaction processes in the reagent mixture, several reaction pathways are incorporated in the kinetic simulation from Table 1. One rate constant is measured, and many others are taken directly from the literature, as indicated in the Table. An important one is the rate constant R1, which uses the published rate constant for the $C_2H + O$ reaction and the published branching ratio to R1. The branching ratio for R2 is reported to be 8%, and it was assumed that 92% of the reaction proceeds through R1. As shown from the surprisal analysis of the CO product of the $C_2H + O$ reaction, the estimate obtained here is not in very good agreement with the previously reported branching ratio. It is noted that the contribution of the $C_2H + SO_2$ reaction to the observed CO(v) product is 20% (approximate estimate) of the removal rate of the $C_2H + SO_2$ reaction, but in the simulation, we assume that all of the $C_2H + SO_2$ reaction results in CO(v); even in this case, the CO from the $C_2H + SO_2$ is still less (see Figure 7) than that from the $C_2H + O$ reaction.

On the basis of the literature of combustion chemistry and experimental observations, four important reactions have been identified that yield CO in the $C_2H_2/C_2H/O/SO_2$ reaction system (R1, R2, R7, R12). Figure 7 shows that, at the concentrations used in our experiment, the CO production is dominated by CO from the $C_2H + O$ reaction at early times. Out of these four reactions yielding vibrationally excited CO, only the $C_2H + O$ reaction shows a quadratic power dependence. This difference in power dependence makes it possible to separate out the CO from the $C_2H + O$ reaction versus all other reactions (see Figure 8). Finally, as already noted, the rise times in the simulations do not agree with the observations, most likely because of a difference in assumed densities in the reaction zone, where a strong pressure and density gradient can occur.

The available energies for R1 and R2 are 28 330 and 5113 cm^{-1}, respectively. From the vibrational distribution, the average fraction of the total available energies released as vibrational energy ($\langle f_v \rangle$) for R1 and R2 are 0.32 and 0.26, correspondingly. The measurements indicate that the CO vibrational distribution is close to the statistical distribution predicted by maximum entropy theory, which would be 0.26 and 0.16, respectively. In addition, the vibrational energy release in these two reactions is somewhat different, suggesting that R2 may be a slightly more direct mechanism than R1. However, it has to be pointed out that the ground vibrational state populations are not known, and the contribution of R2 to $v = 1, 2$ cannot be known independently. This may cause errors in the determination of the vibrational population distributions of R1 and R2. This is especially true for R2, where the ground-state population may be a large fraction of the total populations, and the R1 populations can contribute to $v = 1$ and 2. These factors could bring the results for the $CH(A^2\Delta)/CH(X^2\Pi)$ branching ratio into better agreement with the reported 8% R2 branching fraction. A study is under way to determine the vibrational excitation of the $CH(A^2\Delta)$ state, which should be able to answer this important question. The earlier results could contain some error, such as the yield used for the C_2H or some unaccounted for loss of the C_2H radical, so that the branching ratio may be higher than the 8% reported. To reproduce the earlier determined branching ratio with our results, one would have to assume that the $v = 0$ ground state population from R2 is much less than

the estimate based on the linear surprisal analysis or that the lower vibrational levels from R1 make a much greater contribution. The former would result in a much more inverted vibrational population for CO from R2. It is worthwhile to note that the above discussion assumes that the surprisal is linear and each channel corresponds to one surprisal, which might not be the case (e.g., the $CH(X^2\Pi)$ channel could have a bimodal distribution). The deconvolution procedure is sensitive to the assumed functional form of the vibrational distribution, and parameters extracted may not correspond to the ratios of the $CH(X^2\Pi)$ versus $CH(A^2\Delta)$.

An important question regarding the $C_2H + O(^3P)$ reaction is its mechanism and the possible transition states. Previous studies[22,23] have suggested that the ground state of HCCO[57−59] is the reactive intermediate for the $C_2H + O(^3P)$ reaction for the $CH(A^2\Delta) + CO$ channel. In those studies, the $CH(A^2\Delta) + CO$ channel seems to have surprisingly high importance compared to other possible channels, which is explained through the bent ground state of $HCCO(\tilde{X}^2A'')$. It was suggested that the high nuclear velocities of the $HCCO^{\ddagger}$ may couple to the electronic angular momentum, which is expected to persist in the products, resulting in $CH(A^2\Delta)$ and CO. An explanation for the ground-state $CH(X^2\Pi)$ formation can be as follows: Both the bent $HCCO(\tilde{X}^2A'')$ and its Renner−Teller pair state, the linear $HCCO(\tilde{A}^2\Pi(^2A'))$, have a dissociation limit to the $CH(X^2\Pi)$ state and CO. The linear $HCCO(\tilde{A}^2\Pi(^2A'))$ state can lead directly to $CH(X^2\Pi)$. Also, the linear $HCCO(\tilde{B}^2A')$ state may be formed in the $C_2H + O(^3P)$ reaction, which is known to undergo rapid predissociation (hundreds of picoseconds) to $CH(X^2\Pi)$ and CO.[57,58] Recently, Sattelmeyer et al.[59] investigated the energetics of the five low-lying isomers of the HCCO radical, which may suggest that many possible HCCO isomers contribute to the observed vibrational distribution of CO from R1. The slight preference for energy disposal into the CO vibrations indicates that the energy does not completely randomize in the transition state, which means that the reaction does not proceed through long-lived or multiple transition states, but possibly, there is only one transition state and/or the reaction exit barrier is comparable to the exothermicity of the reaction, putting more energy into translation. The large deviation of the surprisal-predicted branching ratio for R1 and R2 from previous work[22−24] suggests that the CO distribution for R2 could be very different than the surprisal predictions, which might suggest a more direct mechanism.

The results for the $C_2H + O(^3P)$ reaction can be compared to the $CN + O(^3P)$ reaction.[60,61] There are interesting similarities between these two systems. The CN and C_2H have the same number of electrons, and many cases, for example, reactions with hydrocarbons, show comparable reactivity. The CN + O reaction results in $CO + N(^4S)$ and $CO + N(^2D)$ with exothermicities of −77 and −22 kcal/mol, respectively. The $N(^2D)/N(^4S)$ ratio is approximately four. Two things should be noted, which makes comparison of the $C_2H + O$ and the CN + O reaction relevant: (a) Both reactions have the same exothermicity when the products are in their ground electronic states (−77 vs −76.5 kcal/mol). (b) In both reactions, the reaction products can be formed in their electronically excited states, $CH(A^2\Delta)$ for the $C_2H + O$ reaction and $N(^2D)$ for the CN + O reactions. In the zeroth order picture, CH and N can be thought of as a spectator fragment. In this picture, the vibrational distributions of $CO(v)$ could be similar for the formation of the ground electronic state products. The measurements indicate that the $CO(v)$ vibrational distribution for the $N(^4S)$ channel from the CN + O reaction is strongly inverted. The experiments show that the vibrational distribution of $CO(v)$ from the $C_2H + O$ reaction is more statistical ($\langle f_v \rangle = 0.32$) compared to that from the CN + O ($\langle f_v \rangle = 0.5$). The deviation from the zeroth order picture may come from the fact that the $HCCO^{\ddagger}$ complex has a larger number of degrees of freedom compared to the $NCO^{\ddagger}$ complex, resulting in a larger density of states and faster intramolecular vibrational energy redistribution rates. This qualitative comparison is relevant to the $CH(X^2\Pi)$ channel of the $C_2H + O$ reaction, but not to the $CH(A^2\Delta)$ channel, where the difference in exothermicities does not allow such a direct comparison.

Acknowledgment. This work has been supported by the U.S. Department of Energy under the contract #DEAC03-76SF00098. Additional facilities for the kinetic rate determinations were provided by support from the National Aeronautics and Space Administration.

References and Notes

(1) Henkel, C.; Mauersberger, R.; Schilke, P. *Astron. Astrophys.* **1988**, *201*, L23.
(2) Keady, J. J.; Hinkle, K. H. *Astrophys. J.* **1988**, *331*, 539.
(3) Tucker, K. D.; Kutner, M. L.; Thaddeus, P. *Astrophys. J.* **1974**, *193*, L115.
(4) Murphy, J. E.; Vakhtin, A. B.; Leone, S. R. *Icarus* **2003**, *163*, 175.
(5) Pedersen, J. O. P.; Opansky, B. J.; Leone, S. R. *J. Phys. Chem.* **1993**, *97*, 6822.
(6) Chastaing, D.; James, P. L.; Sims, I. R.; Smith, I. W. M. *Faraday Discuss.* **1998**, 165.
(7) Vakhtin, A. B.; Heard, D. E.; Smith, I. W. M.; Leone, S. R. *Chem. Phys. Lett.* **2001**, *344*, 317.
(8) Vakhtin, A. B.; Heard, D. E.; Smith, I. W. M.; Leone, S. R. *Chem. Phys. Lett.* **2001**, *348*, 21.
(9) Carty, D.; Le Page, V.; Sims, I. R.; Smith, I. W. M. *Chem. Phys. Lett.* **2001**, *344*, 310.
(10) Herbst, E.; Woon, D. E. *Astrophys. J.* **1997**, *489*, 109.
(11) Opansky, B. J.; Leone, S. R. *J. Phys. Chem.* **1996**, *100*, 19904.
(12) Opansky, B. J.; Leone, S. R. *J. Phys. Chem.* **1996**, *100*, 4888.
(13) Hoobler, R. J.; Leone, S. R. *J. Phys. Chem. A* **1999**, *103*, 1342.
(14) Hoobler, R. J.; Opansky, B. J.; Leone, S. R. *J. Phys. Chem. A* **1997**, *101*, 1338.
(15) Hoobler, R. J.; Leone, S. R. *J. Geophys. Res., [Planets]* **1997**, *102*, 28717.
(16) Nizamov, B.; Leone, S. R. *J. Phys. Chem. A* **2004**, *108*, 1746.
(17) Lee, S.; Leone, S. R. *Chem. Phys. Lett.* **2000**, *329*, 443.
(18) Boullart, W.; Devriendt, K.; Borms, R.; Peeters, J. *J. Phys. Chem.* **1996**, *100*, 998.
(19) Look, H. V.; Peeters, J. *J. Phys. Chem.* **1995**, *99*, 16284.
(20) Renlund, A. M.; Shokoohi, F.; Reisler, H.; Wittig, C. *Chem. Phys. Lett.* **1981**, *84*, 293.
(21) Renlund, A. M.; Shokoohi, F.; Reisler, H.; Wittig, C. *J. Phys. Chem.* **1982**, *86*, 4165.
(22) Devriendt, K.; Peeters, J. *J. Phys. Chem.* **1997**, *101*, 2546.
(23) Devriendt, K.; Look, H. V.; Ceursters, B.; Peeters, J. *Chem. Phys. Lett.* **1996**, *261*, 450.
(24) Carl, S. A.; Nguyen, H. M. T.; Nguyen, M. T.; Peeters, J. *J. Chem. Phys.* **2003**, *118*, 10996.
(25) Peeters, J.; Langhans, I.; Boullart, W.; Nguyen, H. M. T.; Devriendt, K. *J. Phys. Chem.* **1994**, *98*, 11988.
(26) Shokoohi, F.; Watson, A.; Reisler, H.; Kong, F.; Renlund, A. M.; Wittig, C. *J. Phys. Chem.* **1986**, *90*, 5695.
(27) Segall, J.; Lavi, R.; Wen, Y.; Wittig, C. *J. Phys. Chem.* **1989**, *93*, 7287.
(28) Balko, B. A.; Zhang, J.; Lee, Y. T. *J. Chem. Phys.* **1991**, *94*, 7958.
(29) Segall, J.; Wen, Y.; Lavi, R.; Singer, R.; Wittig, C. *J. Phys. Chem.* **1991**, *95*, 8078.
(30) Hsu, Y. C.; Chen, F. T.; Chou, L. C.; Shiu, Y. J. *J. Chem. Phys.* **1996**, *105*, 9153.
(31) Fletcher, T. R.; Leone, S. R. *J. Chem. Phys.* **1989**, *90*, 871.
(32) *Appl. Spectrosc.* **1993**, *47*(9).
(33) Lauter, A.; Lee, K. S.; Jung, K. H.; Vatsa, R. K.; Mittal, J. P.; Volpp, H. R. *Chem. Phys. Lett.* **2002**, *358*, 314.
(34) Satyapal, S.; Bersohn, R. *J. Phys. Chem.* **1991**, *95*, 8004.
(35) Welsh, H. L.; Stansbury, E. J.; Romanko, J.; Feldman, T. *J. Opt. Soc. Am.* **1955**, *45*, 338.

(36) Atkinson, G.; Parmenter, C.; Schuyler, N. Single Vibronic Level Flourescence. In *Creation and Detection of the Excited State*; Ware, W. R., Ed.; Marcel Dekker: New York, 1971.
(37) Lee, S.; Hoobler, R. J.; Leone, S. R. *Rev. Sci. Instrum.* **2000**, *71*, 1816.
(38) Hsu, Y. C.; Lin, J. J. M.; Papousek, D.; Tsai, J. J. *J. Chem. Phys.* **1993**, *98*, 6690.
(39) Wang, B. S.; Gu, Y. S.; Kong, F. N. *J. Phys. Chem. A* **1999**, *103*, 7395.
(40) Chikan, V.; Leone, S. R. *J. Phys. Chem. A* Submitted.
(41) Fahr, A. *J. Mol. Spectrosc.* **2003**, *217*, 249.
(42) Manatt, S. L.; Lane, A. L. *J. Quant. Spectrosc. Radiat. Transfer* **1993**, *50*, 267.
(43) Ahmed, S. M.; Kumar, V. *J. Quant. Spectrosc. Radiat. Transfer* **1992**, *47*, 359.
(44) Gillespie, D. T. *J. Phys. Chem.* **1977**, *81*, 2340.
(45) Turner, J. S. *J. Phys. Chem.* **1977**, *81*, 2379.
(46) Bunker, D. L.; Garrett, B.; Kleindienst, T.; Long, G. S. *Combust. Flame* **1974**, *23*, 373.
(47) Seki, K.; Okabe, H. *J. Phys. Chem.* **1993**, *97*, 5284.
(48) Opansky, B. J.; Seakins, P. W.; Pedersen, J. O. P.; Leone, S. R. *J. Phys. Chem.* **1993**, *97*, 8583.
(49) Laufer, A. H.; Lechleider, R. *J. Phys. Chem.* **1984**, *88*, 66.
(50) Mantz, A. W.; Maillard, J. P.; Roh, W. B.; Rao, K. N. *J. Mol. Spectrosc.* **1975**, *57*, 155.
(51) Young, L. A.; Eachus, W. J. *J. Chem. Phys.* **1966**, *59*, 4195.
(52) Chandra, S.; Maheshwari, V. U.; Sharma, A. K. *Astron. Astrophys., Suppl. Ser.* **1996**, *117*, 557.
(53) Belikov, A.; Smith, M. *J. Chem. Phys.* **1999**, *110*, 8513.
(54) Alhassid, Y.; Levine, R. D. *J. Chem. Phys.* **1977**, *67*, 4321.
(55) Gong, Y. C.; Makarov, V. I.; Weiner, B. R. *Chem. Phys. Lett.* **2003**, *378*, 493.
(56) Wodtke, A. M.; Lee, Y. T. *J. Phys. Chem.* **1985**, *89*, 4744.
(57) Brock, L. R.; Mischler, B.; Rohlfing, E. A. *J. Chem. Phys.* **1999**, *110*, 6773.
(58) Mordaunt, D. H.; Osborn, D. L.; Choi, H.; Bise, R. T.; Neumark, D. M. *J. Chem. Phys.* **1996**, *105*, 6078.
(59) Sattelmeyer, K. W.; Yamaguchi, Y.; Schaefer, H. F. *Chem. Phys. Lett.* **2004**, *383*, 266.
(60) Holmes, B. E.; Setser, D. W. Physical Chemistry of Fast Reactions. In *Reaction Dynamics*; Smith, I. W. M., Ed.; Plenum Press: New York and London, 1980; Vol. 2.
(61) Shortrid, R.; Lin, M. C. *J. Phys. Chem.* **1974**, *78*, 1451.
(62) Shin, K. S.; Michael, J. V. *J. Phys. Chem.* **1991**, *95*, 5864.
(63) Boullart, W.; Peeters, J. *J. Phys. Chem.* **1992**, *96*, 9810.
(64) Cobos, C. J.; Hippler, H.; Troe, J. *J. Phys. Chem.* **1985**, *89*, 1778.
(65) Zabarnick, S.; Fleming, J. W.; Lin, M. C. *Int. J. Chem. Kinet.* **1989**, *21*, 765.
(66) Bohland, T.; Temps, F.; Wagner, H. G. *Ber. Bunsen-Ges. Phys. Chem.* **1984**, *88*, 1222.
(67) Darwin, D. C.; Moore, C. B. *J. Phys. Chem.* **1995**, *99*, 13467.
(68) Blitz, M. A.; Beasley, M. S.; Pilling, M. J.; Robertson, S. H. *Phys. Chem. Chem. Phys.* **2000**, *2*, 805.